RSC Advances

ROYAL SOCIETY OF CHEMISTRY

www.rsc.org/advances

Journal Name

RSCPublishing

ARTICLE

Cabbage Leaf-shaped TiO_2 Mesostructures for Efficient Dye- sensitized Solar Cells

Cite this: DOI: 10.1039/x0xx00000x

T. G. Deepak[a], G. S. Anjusree[a], K. R Narendra Pai[a], Devika Subash[a], Shantikumar V Nair[a] and A. Sreekumaran Nair*[a]

Received 00th January 2012,
Accepted 00th January 2012

DOI: 10.1039/x0xx00000x

www.rsc.org/

We have fabricated 'cabbage leaf'-like TiO_2 mesostructures of high surface area from electrospun TiO_2-SiO_2 composite nanofibers by titanate route for dye-sensitized solar cell (DSC) application. The initial TiO_2-SiO_2 composite nanofibers, the intermediate titanate and the final leaf-like TiO_2 are characterized by spectroscopy, microscopy and surface area measurements. The material acts (final TiO_2) as a dual functional material in DSCs with high dye loading and a high light scattering capability. The best DSC (a square-shaped cell of area 0.20 cm^2 and thickness of 12 μm) fabricated out of the material showed a superior photovoltaic performance with an efficiency (η) of 7.92% in comparison to that of commercial P25 TiO_2 (6.50%).

Introduction

The pioneering work of O'Regan and Grätzel on dye-sensitized solar cells (DSCs) created a new outlook to solar energy conversion technology which integrated different fields of science.[1] Titanium dioxide (TiO_2) is a versatile and widely used material which has applications in different fields such as photovoltaics, storage devices, photocatalytic water splitting, electrochromic devices, self-cleaning coatings, environmental remediation, etc.[2-13] TiO_2 forms the backbone of the DSCs as it performs the dual functions of supporting the sensitizers (dyes) and transporting the photoinjected electrons to the back contact. The high surface area, smooth charge transport properties (high crystallinity and/or one/two/three-dimensionality) and high light scattering capability of TiO_2 are vital parameters in deciding the photovoltaic performance of DSCs. With these views in mind, different nanostructures have been developed in the past two decades such as nanoparticles,[14-16] nanowires,[17-19] nanotubes,[20-22] nanobelts,[23,24] nanospindles,[25] nanofibers, etc.[26,27] for DSC applications. Except the spherical nanoparticles, all others generally fit into the category of one-dimensional (1-D) nanostructures.

Though there are several methodologies around for the fabrication of 1-D TiO_2, electrospinning is a versatile technique for fabricating TiO_2 in the 1-D form of nanofibers.[28,29] The TiO_2 nanofibers are very good at light scattering as well as in providing a guided/semi-guided electron transport to the back contact. But these materials have shown low conversion efficiency (~4-5 %) due to their low internal surface area and hence poor dye-loading.[30-34] Thus we thought of ways to enhance the surface area of electrospun TiO_2 to have superior DSC performance. The titanate route which is the chemical transformation of spherical TiO_2 nanoparticles into wires/rods by the action of conc. NaOH (first reported by Kasuga et al.[35,36]) was adopted for the purpose as we recently found that the same methodology can produce flower/leaf-shaped TiO_2 from TiO_2-SiO_2 composite nanofibers (the purpose of preparing the composite fibers of TiO_2-SiO_2 was that the SiO_2 can be dissolved by NaOH during the titanate process and etching of SiO_2 from TiO_2-SiO_2 composite leads to enhanced surface area for the TiO_2).[37,38] The flower-shaped material showed excellent photocatalytic properties, however, the photovoltaic property of the TiO_2 was not explored which is the subject matter of the present paper. The initial TiO_2-SiO_2 composites, the intermediate sodium titanate and the final leaf-shaped TiO_2 were characterized by spectroscopy, microscopy and BET surface area measurements. A dye-sensitized solar cell (0.2 cm^2

area, square-shaped, 12 μm thick) fabricated from the leaf-shaped TiO_2 showed an efficiency of 7.92 % when tested under AM1.5G conditions. The cell also showed an incident photon-to-electron conversion efficiency maximum of 79% at 532 nm.

Experimental

a. Materials

PVP (polyvinylpyrrolidone, Mw =1.3×106, mp. 300^0C, Aldrich, Steinhseim, Germany), methanol (Aldrich, Steinhseim, Germany), acetic acid (LR, Nice Chemicals, India), titanium (IV) isopropoxide (TiP, 97%, Aldrich, Germany), tetraethoxysilane (TES, 98% GC grade, Alfa Aesar, UK), sodium hydroxide pellets (A.R, Nice Chemicals, India), hydrochloric acid (ACS, ISO Reag. Ph Eur, Merk KGaA, Germany), N719 dye (Solaronix SA), fluorine-doped tin oxide plates (FTO, sheet resistance of 6-8 Ω/□ fabricated in-house by spray pyrolysis deposition method) were used as such. The precursors of the FTO solution were made of dibutyltin diacetate (DBTDA) in 2-propanol (0.2 M) and ammonium fluoride (NH_4F) in water (9 M).

b. Preparation of cabbage leaf-like TiO_2 mesostructures

Cabbage leaf-like (CL) TiO_2 mesostructures were synthesized from electrospun TiO_2-SiO_2 composite nanofibers. The solution for electrospinning was made by dissolving 0.6 g PVP in 14 mL of methanol. This was followed by the addition of 4 mL of acetic acid (99.7%), 1.75 mL of titanium (IV) isopropoxide and 0.25 mL of tetraethoxysilane, respectively. The mixture was stirred for 12 h to have sufficient viscosity for electrospinning. The mixture was electrospun at 20 kV with a flow rate of 0.5 mL/h using a climate controlled electrospinning unit (IME Technologies, The Netherlands). The distance between the needle tip and the static collector (covered with an Al foil) was about 10 cm. The humidity level inside the electrospinning chamber was maintained at ~ 50%. The as-spun nanocomposite peeled-off from the Al foil in the form of a white sheet was annealed at 450 ℃ for 3 h for polymer degradation and crystallization of the TiO_2-SiO_2 composite. The TiO_2-SiO_2 composite obtained in the form of white flakes was analyzed by microscopy to confirm the nanofiber morphology of the composite.

About 600 mg of electrospun TiO_2-SiO_2 composite nanofibers was chemically treated in excess of concentrated sodium hydroxide (5 M NaOH) at 180 ℃ for 24 h in a Teflon-lined steel autoclave to chemically transform the nanocomposite into titanates with the in-situ etching of SiO_2 completely. The fluffy white titanate was collected and washed repeatedly with Millipore water to have pH=7 for the washed solution. The titanate was subsequently soaked in dil. hydrochloric acid (0.1 M HCl) for 24 h and again washed repeatedly with Millipore water and dried at 180 ℃ for 30 min. During the acid treatment and subsequent drying process, the sodium titanate gets converted into hydrogen titanate and finally into TiO_2. The TiO_2 was characterized by spectroscopy, microscopy and BET surface area measurements.

c. Characterization of the TiO_2-SiO_2 composite, the titanate and the leaf-like TiO_2 material

The annealed TiO_2-SiO_2 nanofibers and the leaf-like TiO_2 were characterized by spectroscopy, microscopy and surface area measurements. The scanning electron microscopy (SEM) was performed by a JSM 6490 LA (JEOL-Tokyo, Japan) machine at an operating voltage at 15 kV. A thin film of gold was sputtered on the material using a sputter coating machine (JEOL-Tokyo, Japan). UV-visible spectra of the TiO_2 thin films (in diffuse-reflectance mode) were measured by a Varian Cary 5000 spectrometer. Transmission Electron Microscopy (TEM) (SEI Tecnai G230) was also carried out for high-resolution imaging. Brunauer-Emmett-Teller (BET) surface area analyzer (Tristar II 3020 Surface Area Analyzer, Micromeritics, USA) was used to analyze the surface area and pore size of the samples, respectively under standard protocol. The powder XRD was performed by an X'pert pro PAN Analytical operated at a data interval of 0.03° and a current of 30 mA with a voltage of 40 KV. X-ray photoelectron spectroscopy (XPS, Kratos Analytical, UK) and Raman spectroscopy (Witec confocal Raman-300 AR instrument using an excitation laser of 488 nm wavelength and power of 0.6 μW, the spot size was > 2 μm) were carried out according to standard procedures.

d. Fabrication of dye-sensitized solar cells (DSCs)

The polyester used to make a paste of TiO_2 was made according to a reported procedure by the polycondesation of citric acid and ethylene glycol at 100 ℃.[31] About 100 mg of the TiO_2 was mixed with 100 μL of the polyester and sonicated for ~ 12 h to get a paste of the right rheology necessary for doctor blading. This was screen-printed/doctor-bladed on FTO plates which already had a blocking layer (80 nm thick) of TiO_2 deposited by spray pyrolysis deposition of a TiO_2 colloid (consisting of ~ 5 nm size particles). The TiO_2 paste was doctor-bladed on FTOs at different thicknesses ranging from14 μm to 20 μm. The P25 was also doctor-bladed similarly for a comparative study. The doctor-bladed films were sintered at 450 ℃ for 1 h for removal of the polymer. The porous TiO_2 films had thicknesses ranging from 12 μm to 18 μm. The porous films were subsequently treated with aq. $TiCl_4$ solution (30 mM, 70 ℃) for 30 min and sintered at 450 ℃ for 1 h. The TiO_2 electrodes were immersed in N719 dye solution (0.5 mM in 1:1 acetonitrile-tert-butanol mixture) at room temperature for 24 h. The weakly adsorbed dyes were removed by washing the electrodes in absolute acetonitrile. Platinum (Pt) sputter-coated FTO was used as the counter electrode. The active area of dye-sensitized TiO_2 was about 0.20 cm^2. The electrodes were sealed with a UV curable sealant and filled with I_3^-/I^- electrolyte (in which, acetonitrile was used as solvent) by vacuum back-filling process using an electrolyte filling robot (SPD Inc. Laboratory, Japan). I-V characteristic of the DSCs was measured by a solar simulator under AM1.5 G condition (Newport Oriel class A-Solar simulator, USA). The incident photon-to-current conversion efficiency (IPCE) was measured using an Oriel Newport (QE-PV-SI/QE) IPCE Measurement kit, USA.

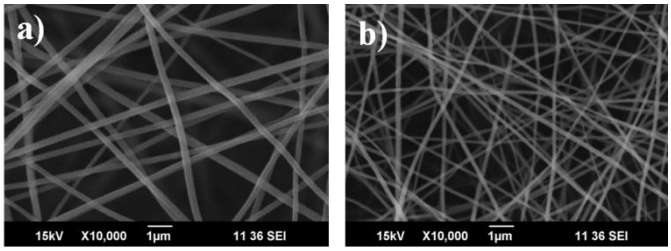

Fig. 1. SEM images of **a)** as-spun TiO_2-SiO_2-PVP fibers and **b)** TiO_2 - SiO_2 nanofibers formed after annealing at 450 ℃.

Electrochemical impedance spectroscopy (EIS) of the DSCs

The electron lifetime and recombination resistance of DSCs were studied using EIS under dark with an applied bias voltage of 0.69 V. In EIS the current response of the cell by applying a small sine wave perturbation was evaluated by using an Autolab (Metrohm, Newport model, Netherlands).

Results and Discussion

a. Characterization of as-electrospun nanofibers, sintered nanocomposite and the leaf-shaped TiO_2.

A SEM image of the as-electrospun TiO_2-SiO_2-PVP composite nanofibers is shown in Fig. 1a. The fibers were smooth and nearly continuous with diameters ranging from 250-300 nm. The as-electrospun nanofibers were sintered at 450 ℃ for 3 h to obtain TiO_2-SiO_2 composite nanofibers with an average diameter of 150 nm (Fig. 1b). The reduction in the fiber diameter is due to the degradation of polymer from the composite matrix. Fig. 2a shows a large area TEM image of the

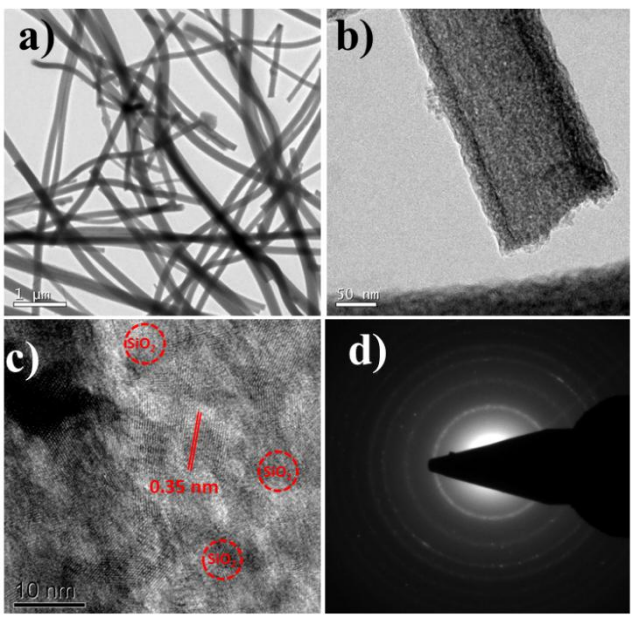

Fig. 2 TEM images of **a)** electrospun TiO_2-SiO_2 nanofiber, **b)** A magnified image of single nanofiber **c)** High-resolution TEM of the TiO_2-SiO_2 nanofiber where unresolved portion shows amorphous SiO_2 and anatase TiO_2 with lattice spacing of 0.35 nm in the composite and **d)** SAED pattern shows polycrystallinity of the composite.

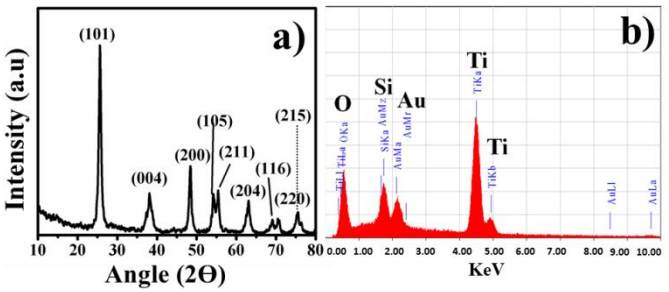

Fig. 3. **a)** Powder XRD spectrum and **b)** EDS spectrum of the TiO_2-SiO_2 composite. The Au signal is from the sputter coating.

TiO_2-SiO_2 composite fibers. Fig. 2b shows a magnified TEM image of a single nanofiber. The high-resolution TEM image (Fig. 2c) indicates the presence of amorphous SiO_2 and anatase TiO_2. The anatase phase of TiO_2 in composite was established by the characteristic lattice spacing of 0.35 nm corresponding to the (101) lattice of anatase (high resolution TEM image in Fig. 2c). The areas (marked in circles) in Fig. 2c indicate the distribution of amorphous SiO_2 in the TiO_2-SiO_2 fibers. The selected area electron diffraction (SEAD) pattern of the TiO_2-SiO_2 nanofibers (Fig. 2d) shows polycrystallinity of the composite.

The TiO_2-SiO_2 composite was further analyzed by powder XRD, BET surface area and XPS measurements, respectively. The prominent peaks in the powder XRD spectrum (indexed in the spectrum itself) of the material confirm the anatase nature of the TiO_2 and amorphous nature of SiO_2 in the composite (Fig. 3a, peaks corresponding to the SiO_2 were absent further confirming its amorphous nature). The presence of Si in the composite was confirmed by energy dispersive X-ray spectrum, EDS (Fig. 3b). The BET surface area of the TiO_2-SiO_2 composite nanofibers was measured to be 32 m^2/g. The XPS survey spectrum showing the elemental composition of the composite material is shown in Fig. 4a and the resolved spectra of the elements are shown in Fig. 4 (b-d). The binding energies

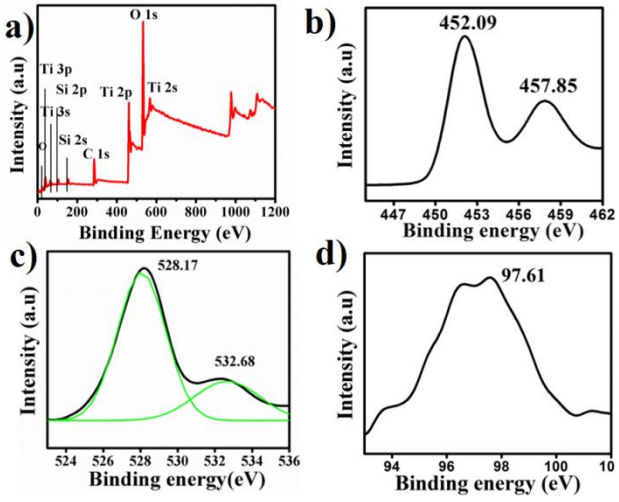

Fig. 4. a) XPS wide spectrum of TiO_2-SiO_2 composite and high resolution spectrum of **b)** Ti **c)** Oxygen **d)** Si.

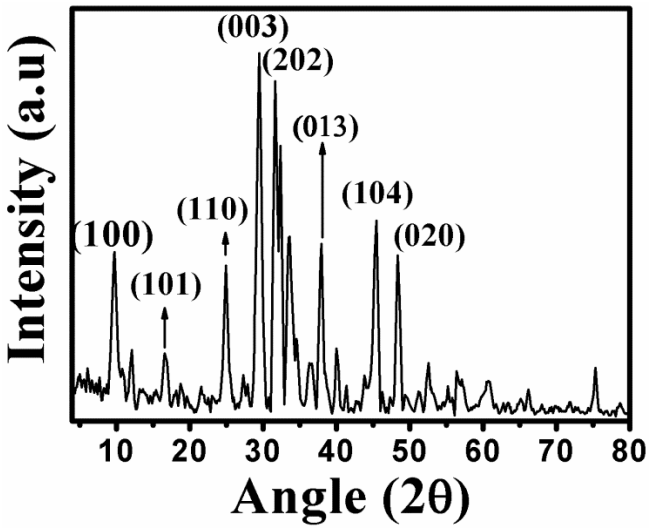

Fig. 5. Powder XRD spectrum of sodium titanate showing a strong peak around **2θ = 10°.** The peaks are indexed in the spectrum itself (JCPDS file no. 72-0148).

for Ti 2p3/2 and Ti 2p1/2 were centered at 452.09 eV and 457.85 eV, respectively (Fig. 4b) that corresponds to a spin-orbit coupling of 5.76 eV. In Fig. 4c, the O1s peak could be de-convoluted into 2 peaks at 528.17 eV, 532.68 eV, respectively, corresponding to the O atom in Ti-O- Ti and Ti-O-Si bonds.[38] Thus, the XPS spectrum indicates the incorporation of SiO_2 in the TiO_2 matrix through Ti-O-Si bonds. The Si peak in the high resolution spectrum (Fig. 4d) is centered at a binding energy 97.61 eV.

The TiO_2-SiO_2 composite obtained by the sintering process upon NaOH treatment results in conversion of TiO_2 into sodium titanate ($Na_2Ti_3O_7$) with the in-situ dissolution of SiO_2. The strong diffraction peak at 2θ = 10° in XRD (Fig. 5) indicates the complete conversion of the composite into titanate.[39.] The XPS spectrum of material (Fig. 6a) after the NaOH treatment (the titanate) confirms complete etching of SiO_2 and the formation of sodium titanate. The binding energies

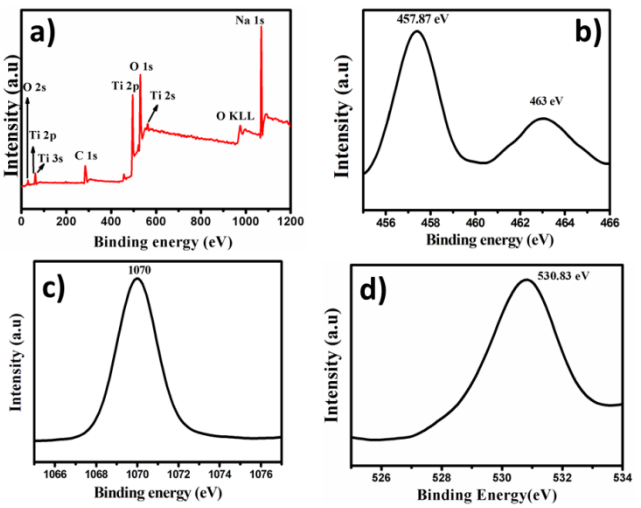

Fig, 6 Fig, 6. **a)** XPS wide spectrum showing complete etching of SiO_2 and presence of Na in the sample. High resolution spectrum of **b**) Ti, **c)** Na and **d)** O.

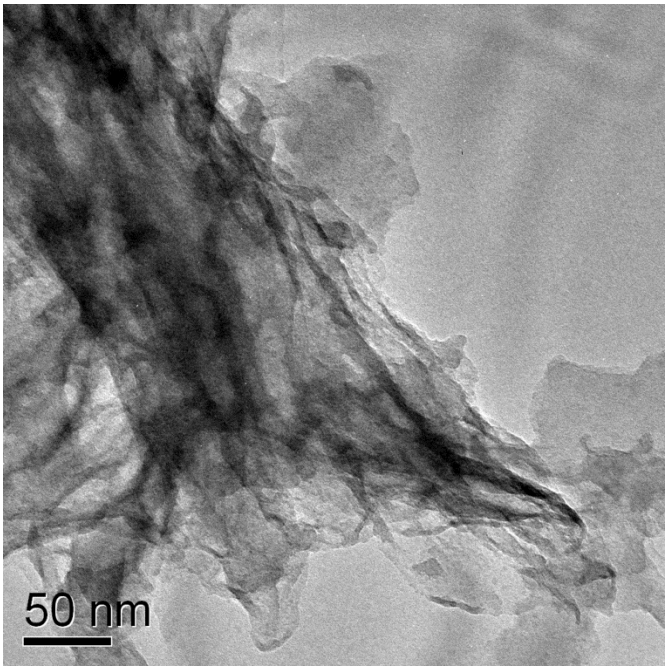

Fig. 7. TEM image of the sodium titanate formed indicating the presence of layered sheet-like structures.

obtained from high resolution spectra of Ti 2p3/2 (centered at 459 eV) and Ti 2p1/2 (centered at 464 eV) reveals that Ti is in a different chemical environment than that of TiO_2 (Fig. 6b). The single peak for O1s at 530 eV represents the O in the Ti-O-Ti bonds (Fig. 6c).[40] The Na 1s peak is obtained at a binding energy of 1072 eV (Fig. 6d). TEM image of the $Na_2Ti_3O_7$ indicated the presence of layered sheet-like structures as evident from Fig. 7.[37,40] The layered and porous nature contributed to a high surface area of 200 m^2/g for the titanate.

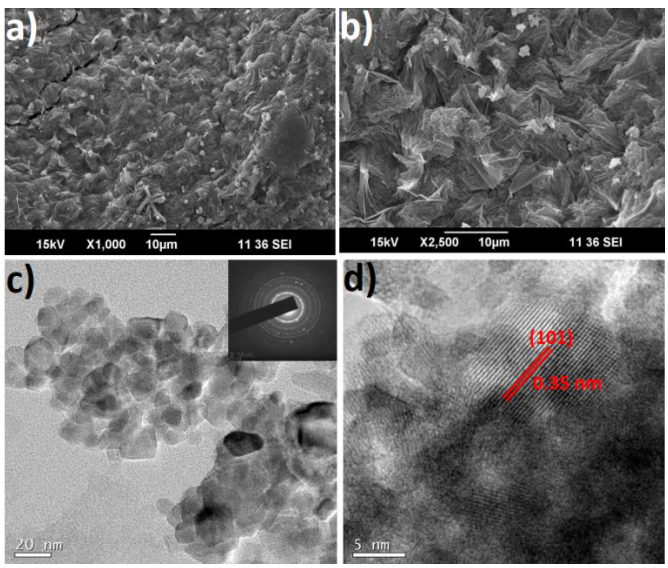

Fig. 8. a) and **b)** SEM image of cabbage leaf-like TiO_2 at different resolutions **c)** HRTEM showing that each petal is composed of nanoparticles of diameter 10-20 nm. **d)** HRTEM showing the lattice spacing of TiO_2.

Further acid treatment and low temperature sintering resulted in the formation of cabbage leaf-like TiO_2 (SEM images in Fig. 8a and Fig. 8b, respectively) possibly through a self-assembly of the sheet-like structures.[37] The BET surface area of the TiO_2 was about 132 m^2/g. High resolution TEM image of a part of the leaf-like structure is shown in Fig. 8c which confirms that the leaf-like TiO_2 is actually made-up of small spherical particles of 10-20 nm sizes. The SAED image (inset of Fig. 8c) reveals the high polycrystallinity of the TiO_2. The lattice-resolved TEM image of the TiO_2 confirms its anatase structure (lattice spacing of 0.35 nm corresponds to the (101) orientation of the anatase TiO_2). Fig. 9a shows the XRD pattern of the leaf-like TiO_2 showing it's crystalline and anatase nature. The peaks are indexed in the spectrum itself. The particle size estimated from the full-width at half maximum of the (101) peak using the Debye Scherrer formula was ~ 12 nm which is in close agreement with the HR-TEM results in Fig. 8c&d. The XPS spectroscopy was also used to confirm elemental composition and phase purity of the TiO_2 (wide spectrum in Fig. 9b). The binding energies of Ti 2p3/2 and Ti 2p1/2 were centered at 456.48 eV and 462.16 eV, respectively (Fig. 9c) corresponding to a spin-orbit coupling of 5.68 eV. The single peak obtained at 527.75 eV for O1s (Fig. 9d) further confirms the absence of SiO_2 related impurities in the final product implying the complete removal of SiO_2 from TiO_2-SiO_2 composite by the action of alkali.

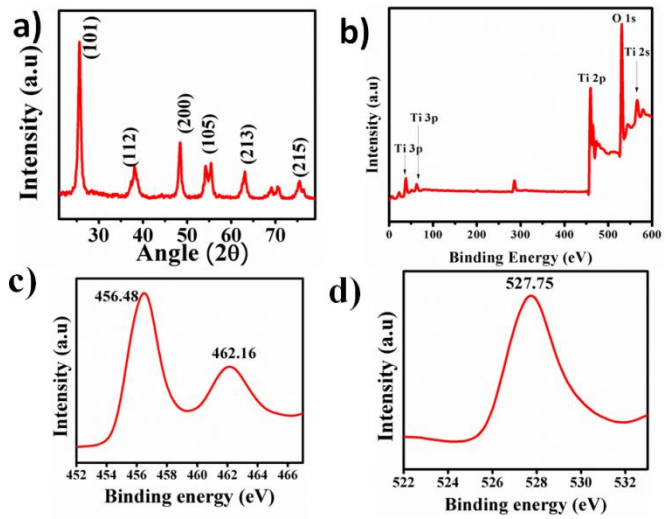

Fig. 9. a) Powder XRD of leaf shaped TiO_2 **b)** XPS Survey spectrum and high resolution XPS spectra of **c)** Titanium and **d)** Oxygen of the TiO_2.

The Raman spectrum of the TiO_2 in Fig. 10 shows the major peaks of anatase TiO_2. The peaks at 404 cm^{-1} and 527 cm^{-1} correspond to the Bg1 and Ag1 vibrational modes, respectively. The other peaks (165cm^{-1}, 207 cm^{-1} and 648 cm^{-1}) observed in the Raman spectrum corresponds to the Eg vibrational mode.[41]

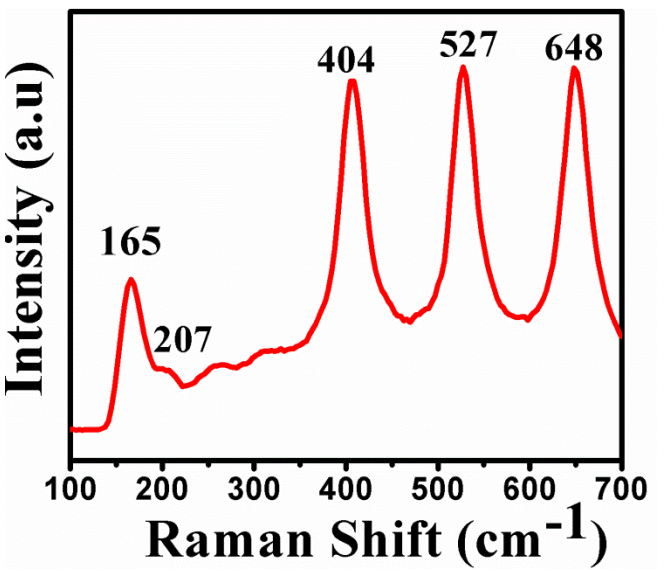

Fig. 10. Raman spectrum of the leaf-shaped TiO_2.

b. Photovoltaic performance of DSCs

The photovoltaic performance of the leaf-like TiO_2 was compared against the commercial P-25 TiO_2 (Fig. 11a). The optimum thickness for best performing DSC was obtained as 11 - 12 µm and the relevant parameters are summarized in Table 1. A conversion efficiency (η) of 7.92 % was obtained with a relatively higher open-circuit voltage (V_{oc}) of 790 mV. The FF of the DSCs was about 74.5% with a current density (J_{sc}) of 13.44 mA cm^{-2}. The photovoltaic parameters of the DSC using P-25 were a J_{sc} of 11.50 mA cm^{-2}, a V_{oc} of 762 mV, a FF of 74.12% and an η of 6.50 %. This is further reflected in the incident photon-to-current conversion efficiency (IPCE) spectra of the DSCs. The IPCE (%) of the DSC employing leaf-like TiO_2 was about 79% whereas the same was only 63% for P-25 employed DSC (Fig. 11b).

A comparison of the PV performance of the two materials indicated that J_{sc} and V_{oc} were the two parameters that contributed to the enhancement of the efficiency for the leaf-like TiO_2. High internal surface area of the material facilitates more dye adsorption on the photoanode film. This is evident from dye deloading data where intensity of dye de-loaded from CL TiO_2 film was considerably higher than that from the P25 TiO_2 film (Fig. 12a). Thus the increase in current density from 11.50 mA cm^{-2} to 13.44 mA cm^{-2} could be partly attributed to the increased dye loading. The other factor that contributes to the current density is the enhanced light scattering by the

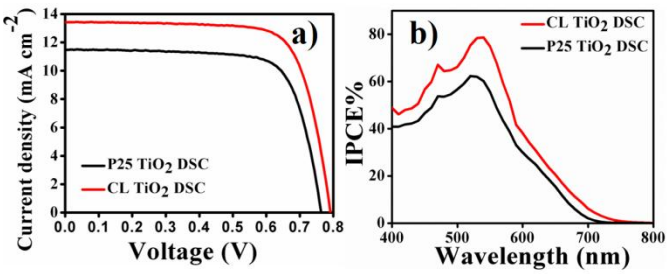

Figure 11. a *J-V* characteristics DSCs of film using CL-like TiO_2 and P-25, **b)** The IPCE (%) of DSCs using P-25 and the CL TiO_2.

Table 1. Thickness dependence PV parameters of the DSCs using the CF TiO_2.

Thickness of the film (μm)	Current density , J_{sc} (mA/cm^2)	V_{oc}	Fill factor (%)	Efficiency, η (%)
10	12.18	0.77	75.02	7.12
12	13.34	0.79	74.53	7.92
15	12.61	0.78	74.23	7.35

mesostructures. Each leaf-like structure of the CL TiO_2 has the overall dimension of 1-2 μm that contributes to enhanced light scattering. A comparison of the reflectance spectra from CL TiO_2 and P25 TiO_2 photoelectrodes is given in Fig. 12b implying high light scattering property of the CL TiO_2. According to the Mie theory, particles with sizes comparable to the wavelength of incident photons scatter light effectively. Light scattering increases the optical path of the light in the photoelectrode which will essentially increase the light interaction with dye molecules (light harvesting efficiency). The IPCE spectrum (Fig. 11b) showed substantial improvement at 650-750 nm wavelength regions (red part of the spectrum) compared to P-25 thus further revealing the contribution from the enhanced light scattering by the leaf-like TiO_2 in the DSC.

The recombination of photoexcited electrons in the conduction band of TiO_2 with the I_3^- ions of the electrolyte is a major loss mechanism in DSCs which determines the overall power conversion efficiency of a DSC device.[42] To have an idea about the effect of morphology on the electron transport, electrochemical impedance spectroscopy (EIS) was performed in both the P-25 and CL TiO_2 DSCs. Parameters such as transport resistance (R_t), Recombination resistance (R_{ct}) and Chemical capacitance (C_μ) in DSCs could be probed through EIS analysis. In the Nyquist plot, the semicircle around 10^1 Hz represents charge transfer at oxide/electrolyte interface.[43] In Fig. 13a, the Nyquist plot shows higher impedance against recombination for the CL TiO_2 DSC that is indicative of lower electron recombination with the I_3^- species in the electrolyte. The recombination resistance (the width of the semicircle at frequency range 10^1 Hz in Nyquist plot) needs to be larger to facilitate charge carriers accumulated in capacitive element to flow through external circuit. In the Bode phase plot (Fig. 13b), phase angle peak corresponds to the electron life time constant

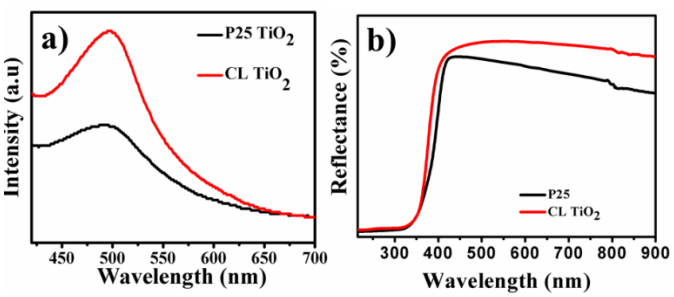

Fig. 12. **Fig. 11**a) The UV-Vis spectra of de-loaded dye from P-25 and CL TiO_2 film in NaOH b) Reflectance spectrum showing enhanced light scattering property of CL TiO_2 especially in the red part of the spectrum.

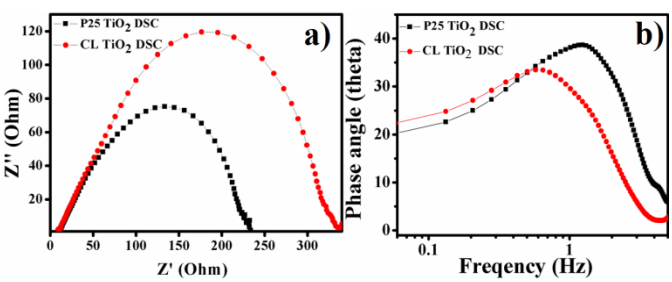

Fig. 13. a) Nyquist plot and **b)** Bode phase plot of DSCs using CL TiO_2 and P25 at dark.

in the TiO_2 film, from which electron life time was estimated using equation $\tau_n=1/(2\pi f)$, where f is the frequency correspond to the phase angle peak. The value of f was shifted from 16.98 Hz (for P-25) to 3.80 Hz (for CL TiO_2). Thus the respective electron lifetimes were found to be 9.37 ms and 41.86 ms, respectively in the two DSCs. The electrons live longer in the CL TiO_2 DSC compared to that in the P-25 TiO_2 film. In short we can attribute high surface area and light scattering property and better charge transport properties possessed by CL-shaped TiO_2 for its superior PV performance over the P-25.

Conclusions

Designing TiO_2 nano/mesostructures with high surface area for dye loading and effective light scattering is a challenge in DSC research; however these are needed for high efficiency DSCs. In this present work we have designed leaf-like TiO_2 mesostructures with high surface area and better light scattering capability through a modified titanate route from TiO_2-SiO_2 composite nanofibers. The initial and final materials were characterized by spectroscopy, microscopy and BET surface area measurements. DSCs employing the leaf-like TiO_2 showed a power conversion efficiency of 7.92% which was ~ 22% higher than that of commercial P-25 (6.5%).

Acknowledgment

Authors thank Ministry of New and Renewable Energy (MNRE), Govt. of India for financial support.

Notes and references

*a Nanosolar Division, Amrita Centre for Nanosciences & Molecular Medicine, Amrita Institute of Medical Sciences, Amrita University, AIMS Ponekkara PO, Kochi 682041, Kerala, India.
Email: sreekumarannair@aims.amrita.edu

1 B. O'Regan and M. Grätzel, *Nature*, 1991, **353**, 737.
2 M. Grätzel, *Nature*, 2001, **414**, 338.
3 A. Hagfeldt and M. Grätzel, *Chem. Rev.*, 1995**, 95**, 49.
4 A. L. Linsebigler, G. Lu and J. T. Yates, *Chem. Rev.*, 1995, **95**, 735.
5 A. Millis and S. Le Hunte, 1997, **108**, 1.
6 P. Zhu, Y. Wu, M.V. Reddy, A.S. Nair, B.V.R Chowdari, and S. Ramakrishna, *RSC Adv.*, 2012, **2**, 531.

7 J. Sundaramurthy, V. Aravindan, P.S. Kumar, S. Madhavi and S. Ramakrishna, *J. Phys. Chem. C*, 2014, DOI: 10.1021/jp412787z.
8 V.J. Babu, M.K. Kumar, A.S. Nair, T.L. Kheng, S.I Allakhverdiev and S. Ramakrishna, *Int. J. Hydrogen Energy* 2012, **37**, 8897.
9 J.B. Veluru, K.K. Manippady, M. Rajendiren, K.M. Mya, P.R. Rayavarapu, S.N. Appukuttan and R. Seeram, *Int. J. Hydrogen Energy*, 2013, **38**, 4324.
10 S. Berger, A. Ghicov, Y.-C. Nah, P. Schmuki, *Langmuir* 2009, **25**, 4841.
11 F. Campus, P. Bonhôte, M. Grätzel, S. Heinen, L. Walder, *Sol. Energy Mater. Sol. Cells*, 1999, **56**, 281.
12 V.A. Ganesh, H.K. Raut, A.S. Nair and S. Ramakrishna, *J. Mater. Chem.*, 2011, **21**, 16304.
13 V.A. Ganesh, S.S. Dinachali, A.S. Nair and S. Ramakrishna, *ACS Appl. Mater. Interfaces* , 2013, **5**, 1527.
14 D.L. Fedlheim, C.A. Foss, *Metal Nanoparticles: Synthesis, Characterization and Applications*, CRC Press: Boca Raton, 2002.
15 T. Sugimoto, *Fine Particles: Synthesis, Characterization and Mechanisms of Growth*, CRC Press: Boca Raton, 2000.
16 M. Grätzel, *Journal of Sol-Gel Sci. and Technol.*, 2001, **22**, 7.
17 C.M. Lieber, Z.L. Wang, *MRS Bull.*, 2007, **32**, 99.
18 K.D. Sattler, *Handbook of Nanophysics: Nanotubes and Nanowires*, CRC Press: Boca Raton, 2011.
19 S. Wang, *Nanowires and Nanobelts: Materials Properties and Devices, Nanowires and Nanobelts of Functional Materials*, Springer-Verlag, 2005.
20 G.K. Mor, K. Shankar, M. Paulose, O.K. Varghese and C.A. Grimes, *Nano Lett.*, 2006, **6**, 215.
21 R. Saito, G. Dresselhaus and M. Dresselhaus, *Physical Properties of Carbon Nanotubes*, Imperial College Press, London, 1999.
22 R.H Baughman, A.A. Zakhidov and W.A. de Heer, *Science* 2002, **297**,787.
23 Z.W. Pan, Z.R. Dai and Z.L. Wang, *Science*, 2001, **291**, 1947.
24 Z.L. Wang, *J. Nanosci. Nanotechnol.*, 2008, **8**, 27.
25 Y. Qiu, W. Chen and S. Yang, *Angew. Chem. Int. Ed.*, 2010, **49**, 3675.
26 S.R. Gajjela, C. Yapa and P. Balaya, *J. Mater. Chem.*, 2012, **22**, 10873.
27 a) Y. Zhou and M. Antonietti, *J. Am. Chem. Soc.*, 2003, **125**, 14960.b) T.G. Deepak, G.S. Anjusree, T. Sara, T.A. Arun, S. V Nair, A.S. Nair, *RSC Adv.*, 2014, **4**, 17615.c) Q. Zhang and G. Cao, *Nano Today.*, 2011, **6**, 91. d) W-Q. Wu, H-S. Rao, Y-F. Xu,Y-F. Wang, C-Y. Su and D-B. Kuang, *Sci Rep.*, 2013, **3,** 1892.
28 D. Li and Y. Xia, *Nano Lett.* 2003, **3**, 555.
29 A.S. Nair, Z. Peining, V.J Babu, Y. Shengyuan and S. Ramakrishna, *Phys. Chem. Chem. Phys*., 2011, **13**, 21248.
30 A.S. Nair, Y. Shengyuan, Z. Peining and S. Ramakrishna, *Chem. Commun.*, 2010, **46**, 7421.
31 A.S. Nair, R. Jose, Y. Shengyuan and S. Ramakrishna, *J. Colloid Interface Sci.,* 2011, **353**, 39.
32 Y. Shengyuan, Z. Peining, A.S. Nair and S. Ramakrishna, *J. Mater.Chem.* 2011, **21**, 6541.
33 M.Y. Song, D.K. Kim, K..J. Ihn, S.M. Jo and D.Y. Kim *Nanotechnology*, 2004, **15**, 1861.
34 H. Kokubo, B. Ding, T. Naka, H. Tsuchihira and S. Shiratori, *Nanotechnology*, 2007, **18**, 165604.
35 T. Kasuga, M. Hiramatsu, A. Hoson, T. Sekino and K. Niihara, *Adv. Mater.*, 1999, **11**, 1307.
36 T. Kasuga, M. Hiramatsu, A. Hoson, T. Sekino, K. Niihara, *Langmuir*, 1998, **14**, 3160.
37 T.A. Arun, D.K. Chacko, A.A. Madhavan, T.G. Deepak, G.S. Anjusree, T. Sara, S. Ramakrishna, S.V. Nair, and A.S. Nair, *RSC Adv.*, 2014, **4**, 1421.
38 A.S. Nair, P. Zhu, V.J. Babu, S. Yang, T. Krishnamoorthy, R. Murugan, S. Peng and S. Ramakrishna, *Langmuir*., 2012, **28**, 6202.
39 E.M. Jr., M.A.S. de Abreu, G.T. Moure, B.A. Marinkovic, P.M. Jardim and A.S. Araujo, *Chem. Mater.*, 2007, **19**, 665.
40 A.S. Nair, Z. Peining, V.J. Babu, Y. Shengyuan, Y. Shengjie and S. Ramakrishna, *RSC Adv.*, 2012, **2**, 992.
41 C.C. Tsai and H. Teng, *Chem. Mater.*, 2006, **18**, 367.
42 J. Bisquert, *J. Phys. Chem. B*., 2002, **106**, 325.
43 K. Park, Q. Zhang, D. Myers and G. Cao, *ACS Appl. Mater.***,** 2013, **5**, 1044.